Influence of holding time during rapid tempering after rapid austenitization on the microstructure and mechanical properties of low carbon steel

Putu Reidita Artha Putri [a,*], Akhmad Ardian Korda [a], Eddy Agus Basuki [a], Fadhli Muhammad [a], Tria Laksana [a], Djalu Amardanta Priambudi [a], Imam Al Syaukhani [a], Septa Berti Santosa [a]

[a] Department of Metallurgical Engineering, Faculty of Mining and Petroleum Engineering, Institut Teknologi Bandung (ITB), Bandung, Indonesia

reiditaarthaputri@gmail.com, korda@itb.ac.id, eddy.a.basuki@itb.ac.id, fadhlim_08@itb.ac.id, tria_laksana@itb.ac.id, djalu13@gmail.com, imam16syaukhani@gmail.com, septaberti@itb.ac.id

(Received 18 September 2025; Accepted 25 February 2026)

Abstract

The rising demand for high-quality steel in construction, automotive, and other industrial sectors presents significant challenges, particularly regarding energy consumption and CO_2 emissions from large-scale production. This study explores the use of rapid tempering as a heat treatment strategy to enhance the mechanical properties of low carbon steel while potentially reducing the environmental footprint of steel manufacturing. Rapid tempering was performed following rapid austenitization at 1000 °C for 90 seconds using a 7-kW induction furnace, followed by quenching in ice water. Soaking times of 5, 15, and 20 seconds were applied during tempering, and results were compared with conventional heat treatment. The rapid tempering process resulted in a microstructure consisting of tempered martensite, with only slight morphological changes in the martensitic phase compared to conventional tempering, and the formation of markedly finer cementite precipitates. Mechanical testing demonstrated superior performance in rapid tempering, with the 5 seconds condition achieving the highest hardness (422.667 HV), tensile strength (1308.9 MPa), and yield strength (1270 MPa), while the 20 seconds condition yielded the highest toughness (139.336 J/cm²) and elongation (33.833%). Based on the balance among tensile strength, hardness, and toughness, the RA-RT 5 seconds specimen exhibited the most optimal mechanical performance.

Keywords: low carbon steel, rapid tempering, rapid austenitization, induction furnace

1. Introduction

Infrastructure development is a key factor in driving economic growth and one of the main aspects of a nation's progress. Steel is one of the primary materials used in infrastructure development due to its superior mechanical properties, such as high strength and load-bearing capacity, making it the material of choice in the construction and manufacturing industries. The World Steel Association projects that global steel demand will reach 1,772 million tonnes in 2025, increasing by 1.2% compared to 2024, equivalent to an additional 21 million tonnes per year [1]. However, large-scale steel production contributes significantly to environmental challenges, with approximately 8% of global CO_2 emissions originating from this sector [2]. According to the International Energy Agency, an average of 1.4 tonnes of CO_2 is emitted for every tonne of steel produced [3].

Conventional quenching and tempering are commonly employed to improve the mechanical properties of steel, particularly toughness and stability [4]. While effective, this process requires relatively long holding times, resulting in high energy consumption. Moreover, in certain applications, achieving the desired strength still requires substantial material usage, indicating room for optimization in microstructural efficiency.

Rapid tempering has emerged as a promising alternative, offering short heating durations compared to conventional tempering. This method promotes the formation of fine and uniform carbide distributions within the ferritic matrix, enhancing the balance of strength, toughness, and ductility [5,6]. It also reduces the risk of tempered martensite embrittlement (TME) and shortens production cycles, thereby improving energy efficiency [7]. The main advantages of rapid tempering include reduced processing times, improved energy efficiency, and enhanced mechanical properties without compromising material toughness [7–9].

By increasing the strength through rapid tempering, steel structures can be designed with reduced thickness or smaller cross-sectional dimensions while maintaining the required load-bearing capacity, resulting in a reduction in total structural mass. This decrease in steel usage directly lowers upstream CO_2 emissions associated with ironmaking, steelmaking, and hot-rolling processes, where emissions scale with the mass of steel produced. Furthermore, the significantly shorter heating times in rapid tempering compared woth conventional tempering reduce thermang energy consumption during heat treatment, enhancing process efficiency. However, research on rapid tempering of low-carbon steels with ultra-short holding times remains limited. Therefore, this study investigates the effects of rapid tempering on the microstructure and mechanical properties of low carbon steel, with comparisons to conventional tempering to evaluate its advantages and limitations.

2. Materials and Methods

Low carbon steel plates (300 × 400 × 6 mm³) supplied by PT Krakatau Steel were used as the test material. The chemical composition was determined using an ARL 3460 optical emission spectrometer. The chemical composition of the studied steel is provided in Table 1. Standard Charpy V-notch (55 × 10 × 10 mm³) and tensile specimens (overall length 110 mm, gage length 12 mm) were machined from the plates.

Table 1. Chemical composition of the studied steel (wt. %)

C	Mn	Si	Ni	Al	Mo	Sn	P	Fe
0.177	0.386	0.138	0.06	0.035	0.037	0.015	0.013	Balance

Two heat-treatment routes were applied: rapid and conventional. Fig. 1 shows the schematic of the heat treatment cycle that was applied. Rapid austenitization was performed in a 7 kW induction furnace at 1000 °C for 90 seconds, followed by ice-water quenching. Rapid tempering was conducted at the same furnace for 5, 15, or 20 seconds, also followed by ice-water quenching. Conventional austenitization was carried out in a muffle furnace at 1000 °C for 30 min, followed by tempering at 200, 400, or 600 °C for 1 hour, with ice-water quenching after each step. Specimen codes reflected the austenitization (RA: rapid austenitization, CA: conventional austenitization) and tempering (RT: rapid tempering, CT: conventional tempering), such that

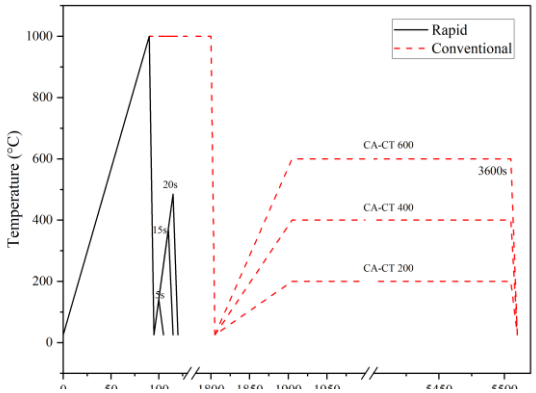

Figure 1. Schematic of the heat treatment parameters applied in this study

CA-CT denotes conventional austenitization followed by conventional tempering, while RA-RT denotes rapid austenitization followed by rapid tempering.

During rapid tempering, the heating rate of the tensile specimens was approximately 23 °C/s, whereas the Charpy specimens experienced an average heating rate of 12.78 °C/s, assuming an initial specimen temperature of 25 °C. The target temperatures corresponding to different holding times for both specimen types are summarized in Table 2.

Table 2. Relationship between holding time and rapid tempering temperature for Charpy and tensile specimens

Holding time (s)	Rapid tempering temperature (°C)	
	Charpy specimen	Tensile specimen
5	88.89	140
15	216.67	370
20	280.56	485

The difference in heating rates and resulting peak temperatures between tensile and Charpy specimens during rapid tempering originates from their distinct geometries and volumes, which lead to different electromagnetic coupling and heat absorption behavior under induction heating. Thinner tensile specimens experience faster heating and reach higher temperatures within the same holding time, whereas the bulkier Charpy specimens heat more slowly. Importantly, both specimen types were subjected to the same nominal holding times during rapid tempering, and the resulting mechanical properties are interpreted based on relative trends within each test method.

Mechanical properties were evaluated by Vickers hardness, tensile, and Charpy impact testing. Vickers hardness measurements were performed on half-Charpy specimens using a NOBEL MHVS-50AT Vickers hardness tester under a HV5 load with a dwell time of 10 s, with hardness values averaged from nine indentations. Tensile tests were conducted at room temperature using a WANCE ETM205 at a crosshead speed of 0.18 mm/min. Impact toughness was determined using a Hung Ta HT-8041 pendulum-type Charpy impact tester at 20 °C, and the absorbed energy was calculated from the pendulum swing angle after fracture.

Metallographic characterization was conducted on half-Charpy specimens from each heat-treatment condition. The specimens were mechanically ground up to 2000# grit, polished using 0.3 μm alumina suspension, etched with 4% nital for 5–10 s, and subsequently examined using field-emission scanning electron microscopy (FE-SEM) to reveal the microstructure. Fractographic analysis was performed on fractured Charpy specimens, which were sectioned from the fracture region, mounted on metal stubs, and also observed by FE-SEM to identify the dominant fracture mechanisms.

3. Result and Discussion

3.1. Mechanical Properties

The mechanical properties obtained from Vickers hardness, tensile tests, and Charpy impact testing are summarized in Table 3. Both increasing tempering temperature in the conventional route and prolonged holding time in rapid tempering resulted in a continuous reduction in hardness, attributable to carbon diffusion from martensite to form carbides and relaxation of dislocation structures [10]. Within their respective processing conditions, rapid tempering produced hardness values comparable to those obtained by conventional tempering, but within significantly shorter processing times. The lowest hardness was recorded in the conventionally

tempered specimen at 600 °C. In contrast, the 5 s rapid tempering specimen produced optimum hardness, demonstrating the effectiveness of short-duration tempering rather than conventional tempering.

Table 3. Mechanical properties of specimens from various heat treatment variations

Variations	Hardness (HV5)	UTS (MPa)	YS (MPa)	Elongation (%)	Impact Energy (J/cm^2)
CA	408.7	1159.7	1112	7.3	27.8
CA-CT 200	393.4	1065.4	1026	10.8	30.3
CA-CT 400	297.7	746.7	740	28.1	118.9
CA-CT 600	219.3	608.9	552	44.8	165.4
RA	434.8	1294.2	1261	18.2	69.1
RA-RT 5s	422.7	1308.9	1270	20.9	75.9
RA-RT 15s	387.1	763.2	712	33.8	101.2
RA-RT 20s	311.4	676.8	600	37.2	139.3

Both UTS and YS followed similar trends. Both conventional and rapid tempering exhibited a decreasing trend as the tempering temperature or holding time increased. Conventionally tempered specimens (CA–CT) reached their highest strength at 200 °C, but the value decreased substantially at higher tempering temperatures, with the lowest strength observed at 600 °C. In contrast, rapid-tempered specimens (RA–RT) achieved the maximum strength at 5 s, but strength declined sharply with longer holding times at 20 s. These results indicate that comparable UTS and YS values can be achieved by RA-RT through a much faster and more energy-efficient process.

Elongation and impact toughness exhibited opposite trends to hardness and strength. Elongation increased with tempering severity, where RA–RT showed relatively low ductility at 5 s but improved with longer holding times, while CA–CT exhibited higher elongation overall, reaching its maximum at 600 °C. This behavior indicates that rapid tempering prioritizes strength over ductility, whereas conventional tempering favors ductility at the expense of strength. Similarly, the Charpy impact data indicated a strong correlation between tempering conditions and toughness. Conventional tempering enhanced toughness progressively with increasing temperature, while rapid tempering was also capable of improving impact toughness in a shorter treatment time. This trend is consistent with the findings of Javaheri et al. (2023) [8], who reported that rapid tempering may reduce tensile strength but simultaneously enhance elongation and impact toughness, thereby providing a better overall mechanical balance. Overall, comparable HV, UTS, YS, and impact thoughness values were achieved via the RA-RT treatment, but through a much faster and more thermally efficient process.

Stress–strain curves (Fig. 2) confirmed the superior performance of rapid tempering. RA–RT at 5 s exhibited the highest tensile strength but limited elongation. With longer holding times (15–20 s), strength decreased while ductility improved due to the development of tempered martensite with globular carbides. In contrast, CA–CT showed lower strength across all conditions, with its optimum at 200 °C and maximum ductility at 600 °C, the latter attributed to extensive softening and carbide coarsening. These results demonstrate that rapid tempering is capable of achieving high strength levels and a competitive strength-ductility balance within significantly shorter processing times compared to conventional tempering.

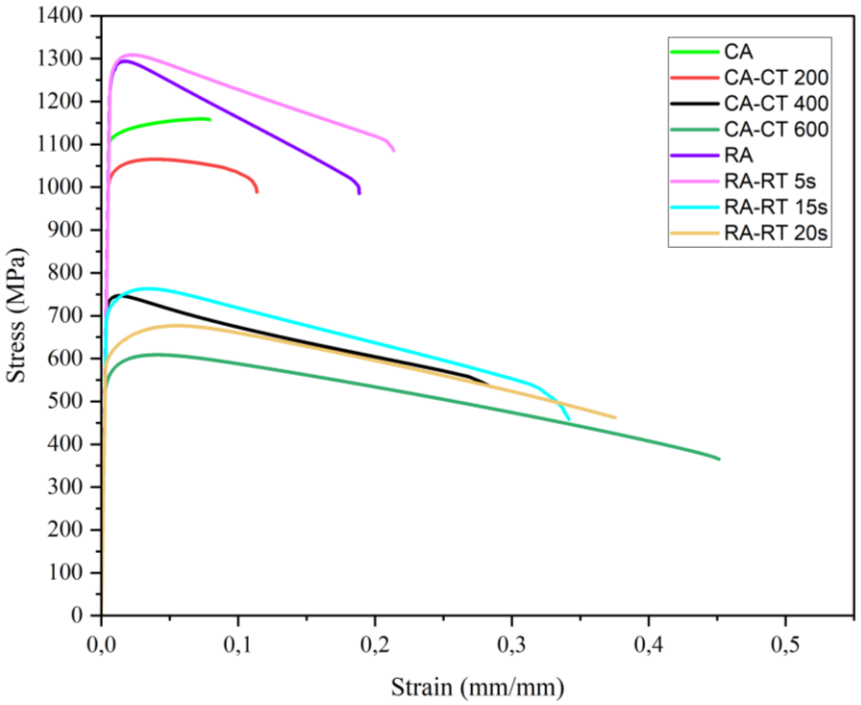

Figure 2. Stress–strain curves of specimens from various heat treatment conditions. Rapid tempering (RA–RT) achieved higher strength at short durations, while conventional tempering (CA–CT) showed greater ductility at elevated temperatures.

Mechanical properties of steels are inherently interrelated, and variations in heat-treatment parameters such as holding time or tempering method simultaneously influence tensile strength, hardness, and toughness. The relationship between tensile strength and toughness is shown in Fig. 3. A general trend was observed where toughness increased at the expense of tensile strength as tempering progressed. The conventionally austenitized specimen (CA) exhibited high tensile strength but low toughness, consistent with its coarse martensitic structure and brittle transgranular fracture. In contrast, specimens subjected to extended tempering, such as CA–CT 600, showed enhanced toughness with reduced strength, characterized by fine dimpled ductile fracture. The most balanced performance was achieved by RA–RT 5s, which reached the highest tensile strength (1308.9 MPa) while maintaining good toughness (75.89 J/cm²). In line with this, Euser et al. (2020) [7] also confirmed that rapid tempering enhanced the impact toughness of AISI 4340 steel compared with conventional treatment. This indicates that short-time rapid tempering effectively retains strength without significantly sacrificing toughness. A similar balance between high strength and improved toughness through rapid tempering was also highlighted by Javaheri et al. (2023) [8] in medium-carbon martensitic steels.

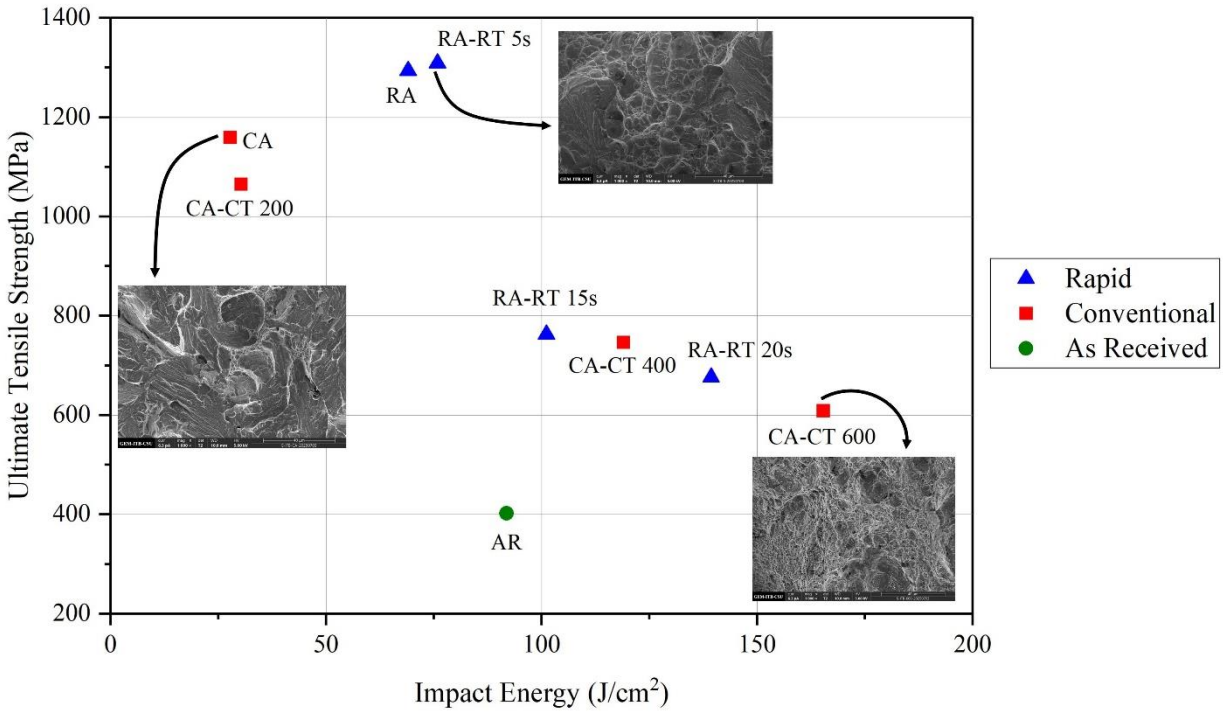

Figure 3. The relationship between ultimate tensile strength and toughness in each experimental variation. Toughness generally increased with tempering at the expense of strength, with RA–RT 5s showing a balanced response.

The Hollomon–Jaffe tempering parameter was employed to quantify the combined influence of tempering temperature and holding time [11]. This relationship, commonly referred to as the Hollomon–Jaffe equation (also known as the Larson–Miller equation), has been presented in various forms by several authors [11–15]. This approach enables the evaluation of tempering conditions in a single parameter, thereby facilitating comparison among different heat treatments. The tempering parameter is represented as:

$$TP = T\,(\log(t) + C) \quad (1)$$

where T is absolute temperature (in Kelvin), t is tempering time (in hour), and C is dependent on the chemical composition of the steel, following the relation $C = 21.3 - (5.8 \times (\text{mass\%C}))$ [16]. The value of C in this experimental steel is taken as 20.

This tempering parameter is used to explain the combined effect of tempering temperature and holding time on the mechanical properties. The application of this parameter is subsequently presented in Fig. 4. The result show that tensile strength decreases with increasing tempering parameters for both tempering methods, primarily due to martensitic softening and transformation into tempered martensite at higher temperatures and holding times. Although partial overlap exists between the two datasets, regression analysis indicates that conventionally tempered specimens achieve slightly higher tensile strength within the same parameter range, suggesting superior performance in this property. In contrast, impact energy increases with increasing tempering parameter and higher values are observed for rapidly tempered specimens. This enhanced toughness may partly originate from the presence of residual ferrite within the sample thickness, resulting from the extremely short austenitization time during rapid heating, which may not allow complete austenite formation throughout the specimen. Such microstructural heterogeneity is consistent with the observed high toughness and elongation, as a fully martensitic structure would typically exhibit lower ductility. However, this explanation is not fully supported by the tensile strength data. As shown in Table 3, the as-quenched RA specimen exhibits significantly higher ultimate tensile strength (1294.2 MPa) than the

conventionally austenitized (CA) condition (1159.7 MPa), indicating that the microstructure is dominated by martensite rather than ferrite. A ferrite-containing microstructure would be expected to reduce UTS rather than increase it.

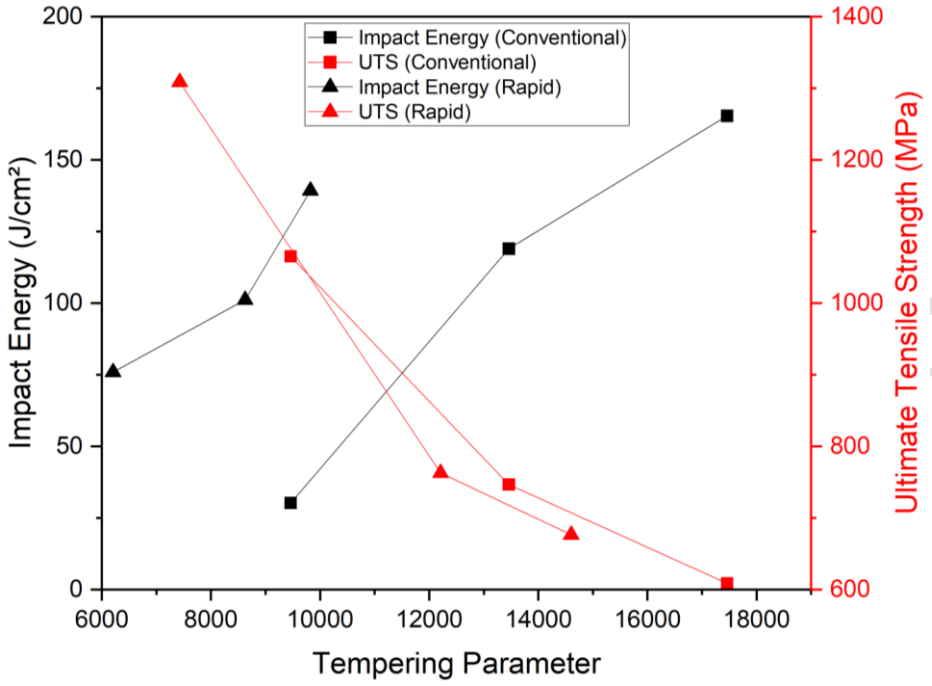

Figure 4. Impact Energy and ultimate tensile strength as a function of tempering parameter for different tempering conditions. Rapid tempering resulted in higher impact energy, while conventional tempering provided slightly higher tensile strength within the same tempering parameter range.

3.2. Microstructural Analysis

SEM-SE observations of the CA specimen in Fig. 5(a), revealed coarse martensitic laths, with some undissolved carbides and inclusions entrapped in the matrix. This is consistent with the diffusionless transformation mechanism, where carbon atoms segregate to dislocations and lath boundaries, while substitutional elements (Mn, Cr, Ni, Mo) remain in supersaturated solid solution, providing potential sites for carbide precipitation during subsequent tempering [17,18]. In the CA-CT 200 specimen (Fig. 5(c)), martensitic laths were still recognizable, although they began to lose their regular alignment and developed into irregular clusters. After tempering at 400 °C, shown in Fig. 5(e), the lath boundaries became increasingly indistinct due to carbide coarsening and the decomposition of retained austenite into coarse cementite along interlath regions [18]. After tempering at 600 °C, as presented in Fig. 5(g), the martensitic morphology almost completely disappeared, being replaced by spheroidized cementite dispersed within an equiaxed ferrite matrix, reflecting Ostwald ripening, where fine carbides dissolve and larger particles grow to reduce interfacial energy [19].

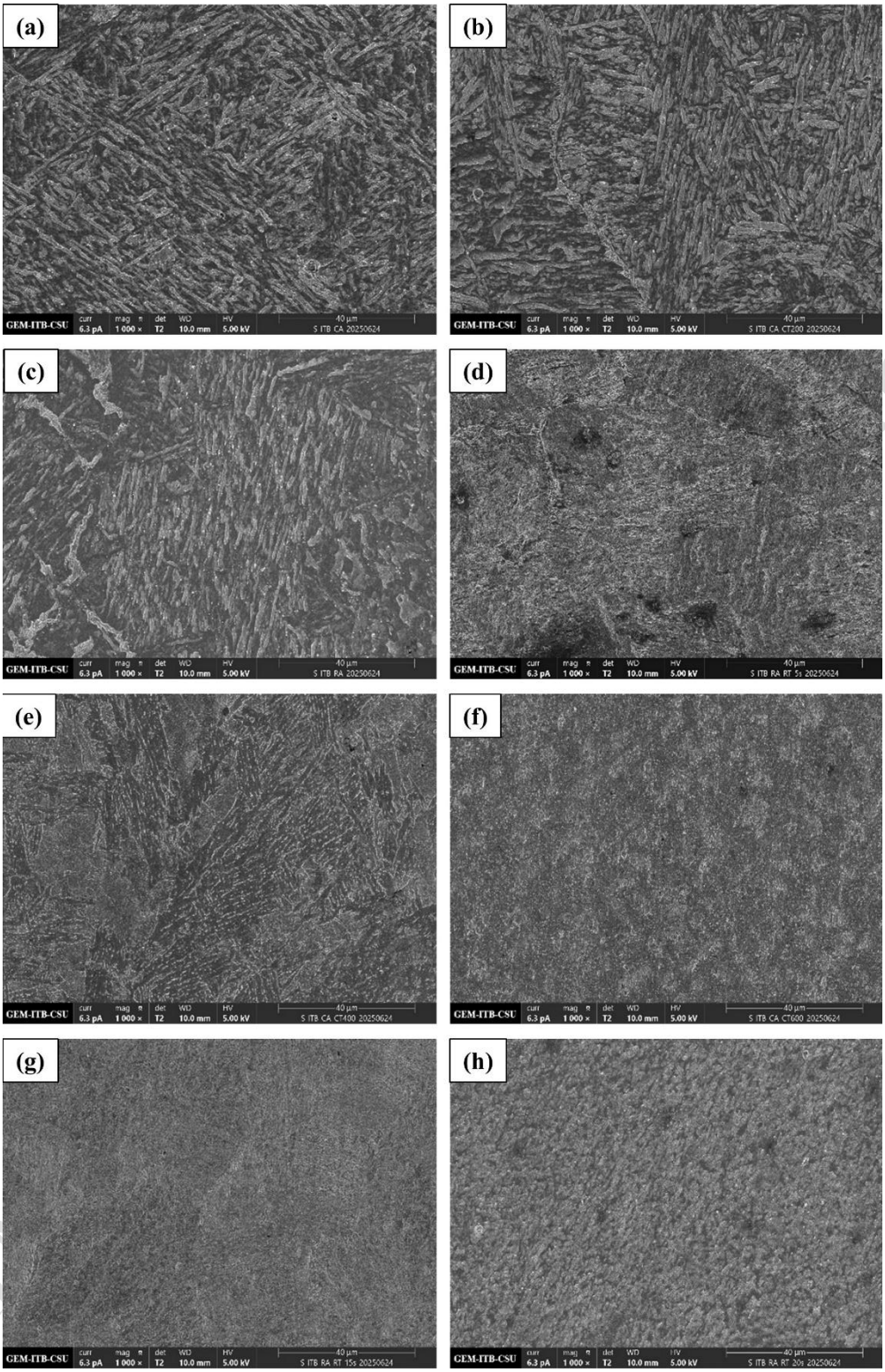

Figure 5. SEM-SE images showing the microstructures of specimens (a) CA, (b) RA, (c) CA-CT 200, (d) RA-RT 5s, (e) CA-CT 400, (f) RA-RT 15s, (g) CA-CT 600, and (h) RA-RT 20s, at 1.000× magnification.

Conventional tempering showed progressive coarsening and spheroidization of carbides, while rapid tempering produced finer and more homogeneous microstructures. Although the SEM-SE images of the as-treated specimens in Figs. 5(a) and 5(b) do not allow a definitive comparison of martensitic lath morphology due to limited magnification, the overall trend of microstructural refinement associated with rapid austenitization is evident after tempering. This refinement

resulted from the extremely short austenitization duration that restricted grain growth [20]. As shown by the paired comparisons of Figs. 5(c)–5(d), 5(e)–5(f), and 5(g)–5(h), RA–RT specimens exhibit a markedly finer and more uniform morphology than their CA–CT counterparts, reflecting the influence of rapid austenitization followed by short-time tempering. This refinement strongly influenced the subsequent tempering response. In the RA-RT 5s specimen, shown in Fig. 5(d), exhibited a less distinct lath morphology, indicating a much finer microstructure and partial softening induced by limited diffusion during rapid tempering. In the RA-RT 15s (Fig. 5(f)) and RA-RT 20s (Fig. 5(h)) specimens, retained smoother and more homogeneous surfaces, reflecting the formation of ultrafine and uniformly distributed cementite, indicating that rapid tempering effectively restricted cementite coarsening [21,22].

Further SEM-SE analysis in Fig. 6(a) confirmed that CA-CT 400 contained partially decomposed laths with cementite precipitation along lath boundaries. In CA-CT 600, martensite was almost fully decomposed into ferrite with dense spheroidized cementite, which was clearly visible at 10,000× magnification as shown in Fig. 6(b). In contrast, the RA-RT 15s specimen in Fig. 6(c) maintained more of its lath morphology, although partial softening was evident with very fine cementite distributed along lath boundaries. In the RA-RT 20s specimen in Fig. 6(d), the lath structure appeared more softened and less defined, while cementite precipitates remained extremely fine and difficult to resolve. Overall, conventional tempering showed progressive carbide coarsening, whereas rapid tempering retained finer lath morphology with ultrafine cementite. These findings demonstrate that short holding times in rapid tempering delay cementite coarsening and promote the retention of refined martensitic features, suggesting an enhanced balance of strength and toughness.

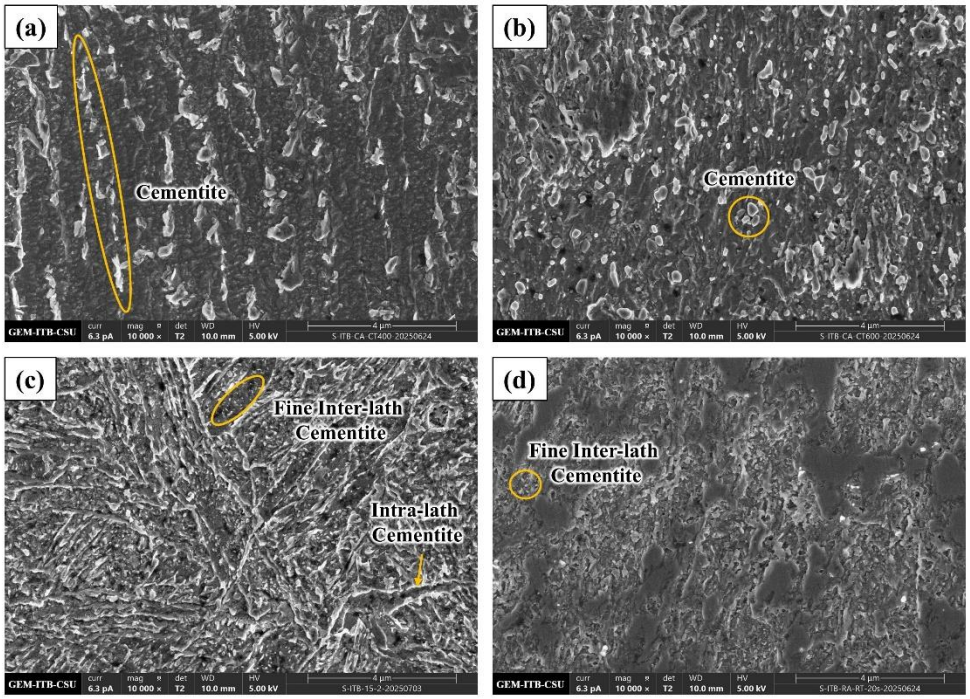

Figure 6. SEM-SE images showing the microstructures of specimens (a) CA-CT 400, (b) CA-CT 600, (c) RA-RT 15s, and (d) RA-RT 20s, at 10,000× magnification.

In conventional tempering, the relatively slow austenitization stage promotes grain growth, resulting in the formation of coarser martensitic laths after quenching. Subsequent tempering mainly drives carbide precipitation (Fe_3C), recovery, and recrystallization at higher temperatures, further modifying the microstructure [23]. In contrast, rapid tempering is preceded by extremely short austenitization, which restricts grain growth and produces much finer martensitic laths. During tempering, only limited carbon segregation and the early formation of very fine cementite

occur, allowing the refined lath morphology to be largely preserved. These distinctions between coarse lath structures in conventional treatment and fine lath structures in rapid treatment are illustrated in Fig. 7.

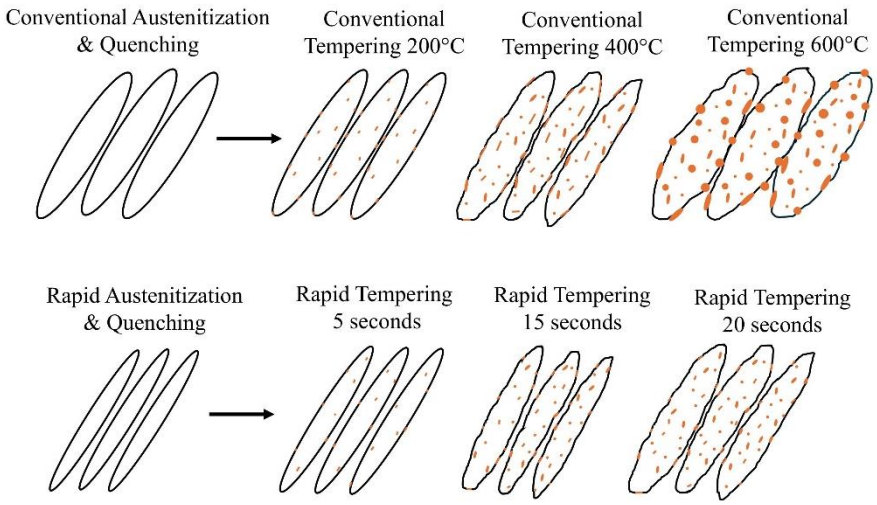

Figure 7. Microstructural illustration after conventional tempering and rapid tempering at different experimental temperatures.

This observation is consistent with Sackl et al. (2016) [6], who reported that cementite in rapidly tempered steels exhibits finer size distribution with a higher particle density, indicating that rapid tempering effectively suppresses excessive cementite coarsening due to the limited diffusion time for carbon atoms. Similarly, Massardier (2014) [24] demonstrated that carbide distribution during rapid tempering is more uniform than under conventional tempering. In conventional tempering, carbide precipitation is typically concentrated along lath boundaries (inter-lath), particularly at higher temperatures, whereas rapid tempering promotes precipitation both within laths (intra-lath) and between laths, yielding a more homogeneous distribution across the martensitic matrix. This pattern reflects the competition between intra-lath nucleation and boundary-driven coarsening. Because rapid tempering delays recovery, the high dislocation density persists and acts as an effective site for intra-lath carbide nucleation. Consequently, nucleation and growth occur concurrently within the short processing time, resulting in a highly uniform precipitation state.

Fracture surfaces of the conventionally austenitized and quenched (CA) specimen were primarily characterized by cleavage and quasi-cleavage facets with faceted transgranular morphology (Fig. 8(a)). Nevertheless, small dimples and microcracks were also present in localized regions. After tempering at 200 °C (CA–CT 200), the fracture surface still exhibited coarse quasi-cleavage features, but these were closely associated with dimples that appeared adjacent to or intersecting the cleavage facets (Fig. 8(c)). This mixed morphology suggests the onset of a transition from brittle to ductile behavior, although cleavage remained the dominant mode. With increasing tempering temperature, the fracture morphology gradually shifted toward ductile behavior. At 400 °C (CA–CT 400), cleavage facets were interspersed with dimples of varying sizes, indicating a mixed fracture mode (Fig. 8(e)). At 600 °C (CA–CT 600), the fracture surface was dominated by uniformly distributed fine dimples, characteristic of microvoid coalescence and extensive plastic deformation (Fig. 8(g)). These features reflect the effect of ferrite recrystallization and cementite spheroidization, which enhance ductility [25].

In contrast, the rapidly austenitized and quenched (RA) specimen displayed a comparatively higher resistance to brittle fracture, although the surface was still dominated by coarse quasi-cleavage and cleavage facets with only limited dimples (Fig. 8(b)). After rapid tempering for 5 s (RA–RT 5s), a mixed morphology emerged, consisting mainly of cleavage facets combined with

a small number of shallow dimples (Fig. 8(d)). Numerous microcracks were also observed across the fracture surface, consistent with the high hardness and tensile strength obtained for this condition, indicating that the material still retained a predominantly brittle character. Extending the tempering time to 15 s (RA–RT 15s) produced a more balanced fracture mode, with numerous coarse and fine dimples (Fig. 8(f)). The longest tempering duration (RA–RT 20s) resulted in a similar fracture morphology, still characterized by coarse and fine dimples, though slightly refined compared with RA–RT 15s (Fig. 8(h)). This subtle refinement is consistent with the modest increase in impact energy relative to the 15 s condition. No significant intergranular fracture was found under any condition.

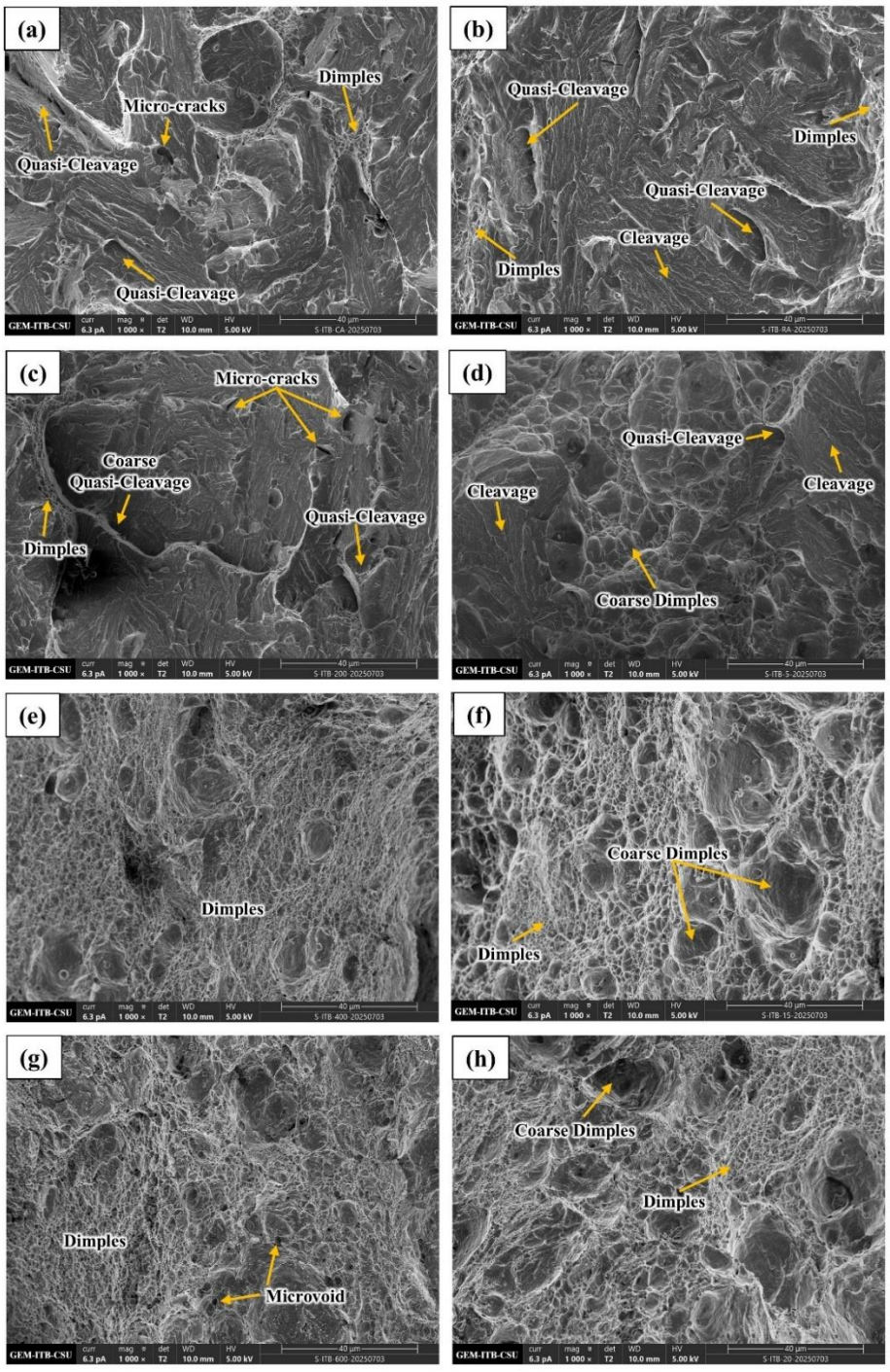

Figure 8. Microfractography of conventionally austenitized and tempered specimens: (a) CA, (b) RA, (c) CA-CT 200, (d) RA-RT 5s, (e) CA-CT 400, (f) RA-RT 15s, (g) CA-CT 600, and (h) RA-RT 20s.

Fractography revealed that RA–RT 5s produced a mixed brittle–ductile fracture surface (Fig. 9, right), unlike the CA–CT 200 °C specimen that remained fully brittle (Fig. 9, left). This difference is linked to the refined martensitic structure formed during rapid austenization, where fine blocks and packets hindered crack propagation by frequent cleavage plane deflection [26,27]. Subsequent 5 s tempering promoted the formation of finely dispersed carbides within and between laths, relieving internal stress without fully softening martensite. These microstructural features caused cleavage cracks to be arrested or deflected, enabling localized microvoid initiation [28]. By contrast, coarser martensite and carbides in CA–CT 200 °C specimens failed to suppress cleavage, resulting in predominantly brittle fracture. Overall, short-time rapid tempering enhanced resistance to crack propagation while retaining much of the strength of as-quenched martensite.

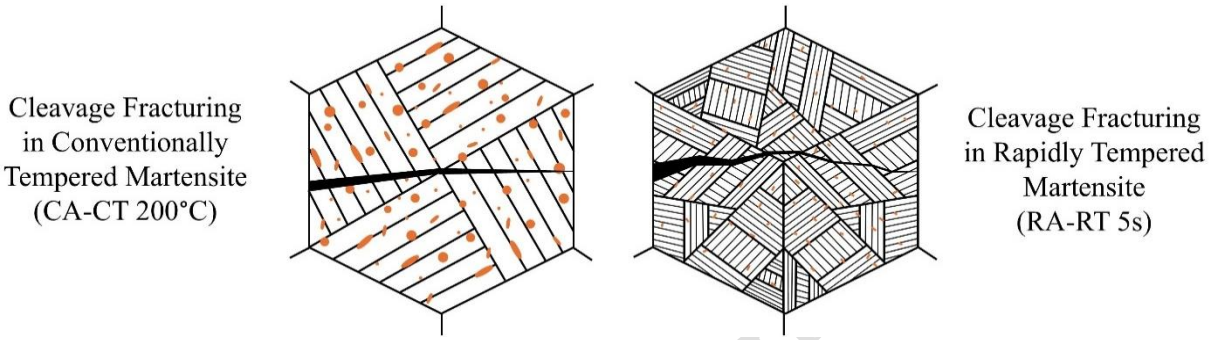

Figure 9. Schematic of crack propagation in the tempering treatment on CA-CT 200 °C (left) and RA-RT 5s (right) specimens.

4. Conclusion

Based on the experimental results and analysis, the following conclusions are drawn:

1. Longer holding times in rapid tempering increased impact energy and elongation, while reducing hardness, tensile strength, and yield strength.
2. Rapid tempering produced a finer microstructure with uniform ultrafine carbide distribution, whereas conventional tempering resulted in coarser ferrite–cementite grains and coarsened carbides. These differences are primarily attributed to the extremely short austenitization and tempering durations in the rapid route, which restricted grain growth and delayed cementite coarsening.
3. Rapid tempering enabled the attainment of a wide range of mechanical properties within very short processing times. The highest hardness (422.667 HV), tensile strength (1308.9 MPa), and yield strength (1270 MPa) were achieved at 5 seconds, while the highest impact toughness (139.336 J/cm²) and elongation (33.833%) occurred at 20 seconds. Considering the balance among tensile strength, hardness, and toughness, the RA-RT 5s condition demonstrated a favorable combination of mechanical properties achieved through a much faster and more energy efficient heat treatment process.

5. Acknowledgement

The authors acknowledge the financial research support from Research, Community Service, and Innovation (PPMI) ITB. The authors also would like to acknowledge the support from GEM-ITB-CSU Joint Research Laboratory for providing the Field Emission - Scanning Electron Microscopy (FE-SEM, Thermo Scientific Apreo 2) used for analysis the samples in this work.

6. Authors Contributions

Putu Reidita Artha Putri: Conceptualization, Methodology, Validation, Formal Analysis, Investigation, Data curation, Visualization, Formal analysis, Writing – original draft, Project administration. Akhmad Ardian Korda: Conceptualization, Methodology, Validation,

Investigation, Writing – review & editing, Resources, Project administration, Funding acquisition. Djalu Amardanta Priambudi: Conceptualization, Methodology, Validation, Investigation, Writing – review & editing. Eddy Agus Basuki: Validation, Investigation, Writing – review & editing. Fadhli Muhammad: Validation, Investigation, Writing – review & editing. Tria Laksana: Validation, Investigation, Writing – review & editing. Imam Al Syaukhani: Validation, Investigation, Writing – review & editing. Septa Berti Santosa: Technical support, assistance with tensile testing and heat treatment.

7. Data Availability

The data presented in this study are available on request from the corresponding author. The data is not publicly available due to privacy.

8. Conflict of interest

The authors declare that they have no known conflicts of interest

9. References

[1] World Steel Association, Short range outlook, (n.d.). https://worldsteel.org/data/short-range-outlook/ (accessed March 11, 2025).

[2] E. Koons, The carbon footprint of steel: decarbonisation is critical, Energy Tracker Asia, (2024). https://energytracker.asia/carbon-footprint-of-steel/ (accessed July 14, 2025).

[3] IEA, Iron & steel, IEA, (2023). https://www.iea.org/energy-system/industry/steel (accessed July 14, 2025).

[4] Y. Zhang, J. Yang, D. Xiao, D. Luo, C. Tuo, H. Wu, Effect of quenching and tempering on mechanical properties and impact fracture behavior of low-carbon low-alloy steel, Metals, 12 (2022) 1087. https://doi.org/10.3390/met12071087.

[5] C. Revilla, B. López, J.M. Rodriguez-Ibabe, Carbide size refinement by controlling the heating rate during induction tempering in a low alloy steel, Materials & Design (1980-2015), 62 (2014) 296–304. https://doi.org/10.1016/j.matdes.2014.05.053.

[6] S. Sackl, M. Zuber, H. Clemens, S. Primig, Induction tempering vs conventional tempering of a heat-treatable steel, Metallurgical and Materials Transactions A, 47 (2016) 3694–3702. https://doi.org/10.1007/s11661-016-3534-3.

[7] V.K. Euser, A.J. Clarke, J.G. Speer, Rapid tempering: opportunities and challenges, Journal of Materials Engineering and Performance, 29 (2020) 4155–4161. https://doi.org/10.1007/s11665-020-04946-z.

[8] V. Javaheri, S. Pallaspuro, S. Sadeghpour, S. Ghosh, J. Sainio, R. Latypova, J. Kömi, Rapid tempering of a medium-carbon martensitic steel: in-depth exploration of the microstructure – mechanical property evolution, Materials & Design, 231 (2023) 112059. https://doi.org/10.1016/j.matdes.2023.112059.

[9] C. Ding, G. Niu, E. Wang, J. Liu, N. Gong, H. Liu, Y. Wang, X. Yu, X. Wang, C. Shang, H. Wu, Significant efficiency improvement of conventional tempering by a novel flash tempering technique, Journal of Materials Research and Technology, 25 (2023) 3551–3560. https://doi.org/10.1016/j.jmrt.2023.06.153.

[10] A.P. Mouritz, Steels for aircraft structures, in: Introd. Aerosp. Mater., Elsevier, 2012: pp. 232–250. https://doi.org/10.1533/9780857095152.232.

[11] J.H. Hollomon,, J.H. Jaffe, Time-temperatures relations in tempering steel, Transactions of the American Institute of Mining and Metallurgical Engineers, 162 (1945) 223–249.

[12] F.R. Larson, J. Miller, A time-temperature relationship for rupture and creep stresses, Journal of Fluids Engineering, 74 (1952) 765–771. https://doi.org/10.1115/1.4015909.

[13] C.R. Manning, Application of rate-temperature parameters to tensile data for magnesium allows and a relation between the Larson-Miller constant and the activation energy, 1960.

[14] E. Pink, Physical significance and reliability of larson–miller and manson–haferd parameters, Materials Science and Technology, 10 (1994) 340–346. https://doi.org/10.1179/mst.1994.10.4.340.
[15] A.K. Sinha, Chapter 14 – tempering, Physical Metallurgy Handbook, McGraw-Hill, New York, 2003.
[16] K. Zhu, X. Zhu, R. Xu, S. Tong, X. Liang, X. Sun, C. Yang, Effect of rapid heat treatment on mechanical properties and precipitation behavior of medium carbon low alloy steel, Journal of Materials Research and Technology, 35 (2025) 5730–5745. https://doi.org/10.1016/j.jmrt.2025.02.206.
[17] G.R. Speich, Tempering of low-carbon martensite, Trans Met Soc AIME, 245 (1969) 2553.
[18] G. Krauss, Tempering of lath martensite in low and medium carbon steels: assessment and challenges, Steel Research International, 88 (2017) 1700038. https://doi.org/10.1002/srin.201700038.
[19] R.A. Oriani, Ostwald ripening of precipitates in solid matrices, Acta Metallurgica, 12 (1964) 1399–1409. https://doi.org/10.1016/0001-6160(64)90128-2.
[20] R.A. Grange, The rapid heat treatment of steel, Metallurgical Transactions, 2 (1971) 65–78. https://doi.org/10.1007/BF02662639.
[21] T. Furuhara, K. Kobayashi, T. Maki, Control of cementite precipitation in lath martensite by rapid heating and tempering, ISIJ International, 44 (2004) 1937–1944. https://doi.org/10.2355/isijinternational.44.1937.
[22] K. Zhu, X. Zhu, R. Xu, S. Tong, X. Liang, X. Sun, C. Yang, Effect of rapid heat treatment on mechanical properties and precipitation behavior of medium carbon low alloy steel, Journal of Materials Research and Technology, 35 (2025) 5730–5745. https://doi.org/10.1016/j.jmrt.2025.02.206.
[23] G. Krauss, Tempering of martensite in carbon steels, in: Phase Transform. Steels, Elsevier, 2012: pp. 126–150. https://doi.org/10.1533/9780857096111.1.126.
[24] V. Massardier, M. Goune, D. Fabregue, A. Selouane, T. Douillard, O. Bouaziz, Evolution of microstructure and strength during the ultra-fast tempering of fe–mn–c martensitic steels, Journal of Materials Science, 49 (2014) 7782–7796. https://doi.org/10.1007/s10853-014-8489-4.
[25] R. Ranjan, A. Meena, Effect of martensite-austenite island decomposition during two-step tempering on the fracture surface morphology of impact and tensile tested mn-ni-mo steel, Engineering Failure Analysis, 161 (2024) 108325. https://doi.org/10.1016/j.engfailanal.2024.108325.
[26] K. Tsuzaki, T. Maki, The effect of cooling rate on the morphology of lath martensite in fe-ni alloys, Journal of the Japan Institute of Metals, 45 (1981) 126–134. https://doi.org/10.2320/jinstmet1952.45.2_126.
[27] F.M. Castro Cerda, B. Schulz, D. Celentano, A. Monsalve, I. Sabirov, R.H. Petrov, Exploring the microstructure and tensile properties of cold-rolled low and medium carbon steels after ultrafast heating and quenching, Materials Science and Engineering: A, 745 (2019) 509–516. https://doi.org/10.1016/j.msea.2018.12.036.
[28] N. Polekhina, V. Osipova, I. Litovchenko, K. Spiridonova, S. Akkuzin, V. Chernov, M. Leontyeva-Smirnova, N. Degtyarev, K. Moroz, B. Kardashev, The cold-brittleness regularities of low-activation ferritic-martensitic steel ek-181, Metals, 13 (2023) 2012. https://doi.org/10.3390/met13122012.